Research Article

A Nondestructive Islanding Detection Method Based on Adaptive and Periodic Disturbance on Reactive Power Output of Inverter-Based Distributed Generation

Xiaolong Chen and Yongli Li

Key Laboratory of Smart Grid of Ministry of Education, Tianjin University, Tianjin 300072, China

Correspondence should be addressed to Yongli Li; lyltju@163.com

In order to detect islanding nondestructively, an islanding detection method for microgrid is proposed based on adaptive and periodic disturbance on the reactive power output of inverter-based distributed generation (DG). The first two parts of the disturbance in a cycle form a symmetric triangular shape and the disturbance can adaptively adjust its peak value and cycle time for two purposes. One is to minimize the total amount of the disturbance. The other is to guarantee that the absolute value of the rate of change of frequency (ROCOF) is constant during islanding, which can be utilized to be a criterion to detect islanding. The method can be applied on the DG either operating at a unity power factor or generating both active and reactive power simultaneously. Moreover, it helps to avoid the serious transient process during control strategy transformation of the DG for microgrid islanded operation. According to the anti-islanding test system in the IEEE Std. 929-2000 and IEEE Std. 1547-2003, several study cases are carried out in the PSCAD/EMTDC environment. The simulation results show that the proposed method can detect islanding rapidly and nondestructively. Moreover, it also performs effectively for the system with multiple DGs.

1. Introduction

The inverter-based distributed generation (DG) uses renewable energy such as wind power, photovoltaics, and microturbine to supply power [1]. It is being widely researched and applied to meet the targets of environmental protection and harmonious development of the power industry. Microgrid usually contains the DG, the load, and control devices based on a certain topology structure [2–4]. It can realize the effective management of the DG and fully mine its value for the benefits of both the grid and users [5, 6].

Islanding is a condition in which a portion of the utility system that contains both the DG and load continues operating while this portion is electrically separated from the main utility [7, 8]. There are two types of islanding: (1) intentional islanding and (2) inadvertent islanding. According to the control strategy in advance, intentional islanding forms in a controlled manner to make good use of the DG and improve the power supply reliability [8, 9]. This operation mode is not studied in this paper. On the contrary, inadvertent islanding can lead to power quality problems,

serious equipment damage, and even safety hazards to utility operation personnel [10]. Therefore, the DG has to detect islanding rapidly and effectively in this case to prevent the damage mentioned above.

Generally, the islanding detection methods can be mainly classified into three categories: (1) passive methods; (2) active methods; and (3) communication-based methods. Communication-based methods rely on power line carrier communications and do no harm to the power quality of the power system with the negligible nondetection zone (NDZ), but the cost is much higher than the other two types of methods and the operations are more complex as well [11]. Therefore, passive and active methods have been well developed.

Passive methods determine the islanding condition by measuring system parameters such as magnitude of the voltage at the point of common coupling (PCC), the PCC voltage frequency, and phase jump [12]. Over/underfrequency protection (OFP/UFP) and over/undervoltage protection (OVP/UVP) are the most widely used passive islanding detection methods. According to GB/T 19939-2005 (China),

the voltage thresholds are typically set at 0.85 pu and 1.1 pu, while the frequency thresholds are set at 49.5 Hz and 50.5 Hz (50 Hz is the rated frequency of the power system) [13]. Passive methods are easy to implement and do no harm to the power quality of the power system, but they may fail to detect islanding when the local load consumption closely matches the power output of the DG [14].

In order to reduce or eliminate the NDZ, active methods rely on injecting intentional disturbances or harmonics into some DG parameters to identify whether islanding has occurred [15–17]. Active methods mainly include the active frequency drift (AFD), slip-mode frequency shift (SMS), and Sandia frequency shift (SFS) methods, which can create a continuous trend to change the frequency during islanding [18–20]. Though active methods suffer smaller NDZs, the presence of disturbances during normal operation will sacrifice power quality and reliability of the power system. Moreover, some active methods have difficulty in maintaining synchronization of the intentional disturbances. Therefore, they may not work owing to the averaging effect when applied in multiple-DG operation [21, 22].

Islanding detection methods based on reactive power control are more attractive. With the designed reactive power reference for the DG, these methods can be easily implemented. The NDZ can be reduced or even eliminated with proper design. Moreover, these methods do not cause current distortion during the normal operation [23].

An islanding detection method relying on equipping the DG interface with a Q-f characteristic was proposed in [24]. It was hard to guarantee that the slope of the DG Q-f curve, which was a preset and fixed value, would be steeper than that of the load curve. Thus, the method might fail to detect islanding in some cases. Reference [25] presented an islanding detection method based on intermittent bilateral reactive power variation and the frequency was forced to deviate to the thresholds during islanding. Compared with the method in [25], the proposed method in [26] was improved by only generating unilateral reactive power variation in each variation period and reducing the reactive power output based on the load's resonance frequency. However, if the islanding occurred when the reactive power variation was equal to zero, it would not be detected rapidly with the detection time probably up to a whole variation cycle 1.8 s. Moreover, when the methods were applied to multiple DGs, the synchronization of the reactive power variation might not be guaranteed and the methods would fail to detect islanding.

The methods in [24–26] were designed for the DG operating at a unity factor during the normal operation. However, the DG was also explored to compensate reactive power simultaneously for power factor improvement [27, 28], as well as the voltage regulation [29, 30]. The method in [31] was designed for this kind of DG. With the designed reactive power reference, the DG continuously and partly compensated the load reactive power consumption, thus forcing the frequency to rise or drop until the frequency deviated outside the OFP/UFP limits. However, the detection speed varied and it would be too slow if the load consumed little reactive power.
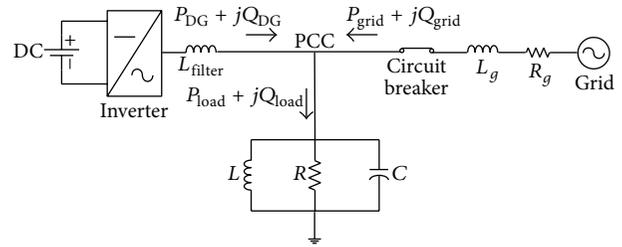

Figure 1: The recommended generic system for islanding study.

Most active methods aim to force the frequency to deviate outside the OFP/UFP limits to detect islanding. However, the abnormal frequency after detection makes the control strategy transformation of the DG for microgrid islanded operation hard. Therefore, a nondestructive islanding detection method for microgrid is proposed in this paper. The method relies on the periodic disturbance on the reactive power output of the DG. The disturbance in a cycle has three parts with equal duration and the first two parts of the disturbance form a symmetric triangular shape. Accordingly, the frequency deviates in a symmetric triangular shape without exceeding its limits. In addition, the disturbance in the next cycle can adaptively adjust its peak value and cycle time according to the frequency in the third part of the disturbance in last cycle. The design is for two purposes: (1) minimizing the total amount of disturbance and (2) making sure that the absolute value of the ROCOF is constant during islanding, which can be utilized to be a criterion to detect islanding. The method has the universal nature. It can be applied on the DG either operating at a unity power factor or generating both active and reactive power simultaneously. Moreover, it performs effectively as well for the system with multiple DGs. Due to the method's nondestructive effect on the frequency, it helps to avoid the serious transient process during control strategy transformation of the DG for microgrid islanded operation.

2. Recommended Generic System Modeling and Basic Relationship Analysis

2.1. Recommended Generic System for Islanding Detection. As shown in Figure 1, a generic system for islanding detection study is recommended according to the IEEE Std. 929-2000 and IEEE Std. 1547-2003. It consists of an inverter-based DG, a parallel three-phase RLC load, and the distributed network represented by a three-phase source behind impedance. When the breaker is open, the DG and its local load are disconnected from the distributed network and islanding can be simulated.

Active methods aim to detect islanding when the local load consumption closely matches the DG output power. Due to the fact that the detection time is short, the DG output power can be considered to be constant during the detection. Therefore, using a constant dc source behind a three-phase
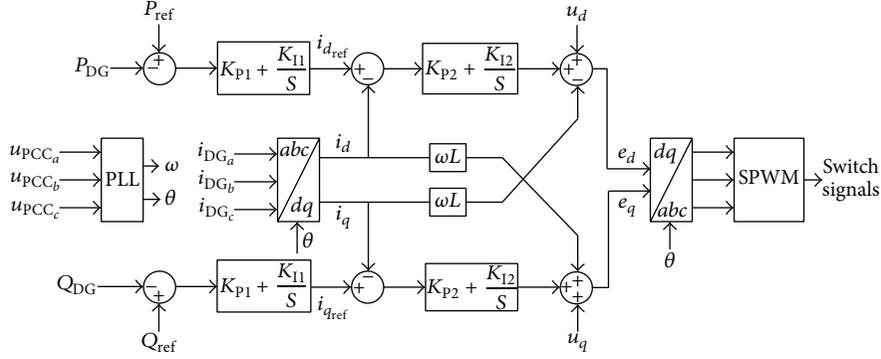
FIGURE 2: The block diagram of the DG interface control.

inverter, the DG is usually designed as a constant power source.

Based on the dual close loop control structure in the d-q synchronous reference frame, the DG can control the active and reactive power output independently. The block diagram of the DG interface control is shown in Figure 2. It mainly contains the phase-locked loop (PLL), the outer power control loop, and the inner current control loop. The PLL offers the voltage phase angle as a benchmark phase to realize synchronous Park transformation. In addition, it can calculate the frequency of the PCC voltage as well, which can be utilized to judge whether islanding occurs or not according to the OFP/UFP. In the outer power control loop, according to PI regulators, the errors between active and reactive power output of the DG and their preset values are transformed into the reference values of active and reactive current, respectively. In the inner current loop, the errors between the measured and reference d-q values of the DG current are also passed through PI regulators. Meanwhile, the feed-forward compensation from the d-q voltages at the PCC realizes the decoupled control of the d-q components of the DG current as well as the DG active and reactive power output. According to the Park transformation, the output of the inner current control loop is transformed into the reference values of the output voltage of the DG. Then, the triggering pulses on the inverter switches are gained by sinusoidal pulse-width modulation (SPWM).

The instantaneous active and reactive power output of the DG can be written in terms of the d-q axis components as follows [32]:

$$P_{\mathrm{DG}} = \frac{3}{2} u_d i_d$$
$$Q_{\mathrm{DG}} = \frac{3}{2} u_d i_q, \tag{1}$$

where u_d and u_q represent the d-q components of the PCC voltage and i_d and i_q are the d-q components of the DG current. Under the balanced network conditions, the abovementioned d-q components are constant.

2.2. Basic Relationship Analysis.
When the DG and its local load are connected to the utility grid, the power flows and the active and reactive power consumed by the RLC load can be expressed as follows:

$$P_{\mathrm{Load}} = P_{\mathrm{DG}} + P_{\mathrm{Grid}} = 3 \frac{V_{\mathrm{PCC}}^2}{R} \tag{2}$$

$$Q_{\mathrm{Load}} = Q_{\mathrm{DG}} + Q_{\mathrm{Grid}} = 3 V_{\mathrm{PCC}}^2 \left(\frac{1}{2\pi f L} - 2\pi f C \right), \tag{3}$$

where RLC represent the load resistance, inductance, and capacitance and V_{PCC} and f are the root mean square (RMS) of the single-phase voltage at the PCC and its frequency, respectively. In addition, (3) can also be written in terms of the RLC load's resonant frequency (f_0) and quality factor (Q_f) as follows [26]:

$$Q_{\mathrm{Load}} = P_{\mathrm{Load}} Q_f \left(\frac{f_0}{f} - \frac{f}{f_0} \right) \tag{4}$$

and the f_0 and Q_f can be expressed as follows:

$$f_0 = \frac{1}{2\pi \sqrt{LC}}$$
$$Q_f = R \sqrt{\frac{C}{L}} = 2\pi f_0 R C. \tag{5}$$

It can be inferred from (2) that when islanding occurs, the PCC voltage falls or rises according to the active power mismatch ΔP ($\Delta P = P_{\mathrm{Load}} - P_{\mathrm{DG}}$). If the active power of the DG is set constant, the active power mismatch can be expressed as follows [33]:

$$\Delta P = P_{\mathrm{DG}} \left(\frac{1}{(1 + \Delta V)^2} - 1 \right) \tag{6}$$

and ΔV can be expressed as

$$\Delta V = \frac{V_{\mathrm{PCC}}^* - V_{\mathrm{PCC}}}{V_{\mathrm{PCC}}}, \tag{7}$$

where V_{PCC} and V_{PCC}^* represent the PCC voltage before and after islanding, respectively.

If the DG operates at a unity power factor, the reactive power consumed by the local load will be equal to zero after islanding. Therefore, the value of the frequency after islanding is equal to that of f_0 according to (4). In order to force the frequency after islanding to deviate to a certain value (such as 50 Hz or the frequency threshold values 50.5 Hz and 49.5 Hz), the additional amount of the reactive power can be derived according to (4) as follows:

$$
\begin{aligned}
\Delta Q_1 &= Q_1 - Q_{\text{DG1}} = P_{\text{DG}} Q_f \left(\frac{f_0}{f_{\text{tar}}} - \frac{f_{\text{tar}}}{f_0} \right) - 0 \\
&= P_{\text{DG}} Q_f \left(\frac{f_1}{f_{\text{tar}}} - \frac{f_{\text{tar}}}{f_1} \right),
\end{aligned}
\tag{8}
$$

where f_{tar} represents the target value of frequency, Q_1 is the reactive power with the frequency equal to f_{tar}, and f_1 represents the frequency after islanding with its value equal to that of f_0 in this case.

On the other hand, if the DG generates both active and reactive power simultaneously, the value of f_1 depends on both active and reactive power mismatches [34]. In order to force the frequency after islanding to deviate to its threshold in this case, the additional amount of the reactive power can be derived as

$$
\begin{aligned}
\Delta Q_2 &= Q_2 - Q_{\text{DG2}} \\
&= 3 V_{\text{PCC}}^{*2} \left(\frac{1}{2\pi f_{\text{tar}} L} - 2\pi f_{\text{tar}} C \right) \\
&\quad - 3 V_{\text{PCC}}^{*2} \left(\frac{1}{2\pi f_1 L} - 2\pi f_1 C \right) \\
&= P_{\text{DG}} Q_f \left(f_1 - f_{\text{tar}} \right) \left(\frac{f_0}{f_1 f_{\text{tar}}} + \frac{1}{f_0} \right),
\end{aligned}
\tag{9}
$$

where Q_2 is the reactive power with the frequency equal to f_{tar} for the DG of this kind. Since the change of f_0 around 50 Hz has negligible impact on the value of ΔQ_2, f_0 could be set as 50 Hz and (9) can be rewritten as follows:

$$
\Delta Q_2 = P_{\text{DG}} Q_f \left(f_1 - f_{\text{tar}} \right) \left(\frac{50}{f_1 f_{\text{tar}}} + \frac{1}{50} \right).
\tag{10}
$$

On the basis of islanding detection standards, the power factor Q_f of the RLC load is set as 2.5. Assuming that P_{DG} is equal to 1, Figure 3 illustrates the relationship between f_1 and ΔQ when f_{tar} is set as 50 Hz and the threshold values 49.5 Hz and 50.5 Hz according to (8) and (10). It can be seen from Figure 3 that (1) no matter whether the DG operates at a unity factor or generates active and reactive power simultaneously, the ΔQ-f_1 curves are the same; (2) the ΔQ-f_1 curves show the approximately linear characteristic for the period between 49.5 Hz and 50.5 Hz; (3) when f_1 is greater than or equal to 50 Hz, the additional reactive power can be calculated with
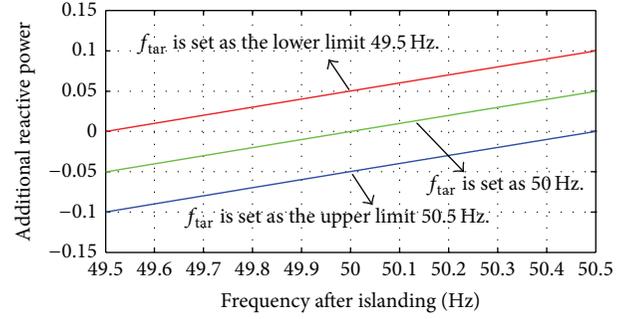

FIGURE 3: The ΔQ-f_1 curves when f_{tar} is set as 50 Hz and the threshold values.

f_{tar} equal to 50.5 Hz. And the additional reactive power can be calculated with f_{tar} equal to 49.5 Hz when f_1 is smaller than 50 Hz. Therefore, the additional reactive power is within $\pm 5\%$ P_{DG}.

3. Proposed Nondestructive Islanding Detection Method Based on Adaptive and Periodic Disturbance on the Reactive Power Output of the DG

Traditional active methods usually force the frequency to deviate outside the OFP/UFP limits to detect islanding. However, the abnormal frequency makes the control strategy transformation of the DG for microgrid islanded operation hard. In this paper, a nondestructive islanding detection method for microgrid is proposed, which can keep the frequency in the normal operating range and avoid the serious transient process during the control strategy transformation of the DG.

It can be seen from (6), (8), and (10) that the active power mismatch makes the voltage change after islanding, while the frequency variation depends on the reactive power mismatch no matter whether the DG operates at a unity power factor or generates active and reactive power simultaneously. Thus, periodic disturbance on the reactive power output of the DG can be utilized to detect islanding. In addition, islanding should be detected rapidly with the minimum reactive power disturbance. Therefore, the proposed method includes three key points: (1) maintaining the frequency in the normal operating range; (2) designing proper criterions to detect islanding rapidly; and effectively (3) minimizing the total amount of the disturbance by adaptively adjusting its peak value and cycle time.

According to the study on the relationship between the reactive power mismatch and the frequency variation after islanding in Section 2, the ΔQ-f_1 curve shows the approximately linear characteristic for the period between 49.5 Hz and 50.5 Hz. Therefore, the disturbance in a cycle is designed to be divided into three parts with equal duration and the first two parts form a symmetric triangular shape. Accordingly, the frequency deviates in a symmetric triangular shape without exceeding its limits after islanding when the periodic disturbance is added on reactive power output of

the DG. The reactive power disturbance in a complete cycle can be expressed as follows:

$$\Delta Q_{dis} = \begin{cases} \dfrac{\Delta Q_{peak}}{(1/3)\,T}t, & 0 \leq t < \dfrac{1}{3}T \\ \dfrac{\Delta Q_{peak}}{(1/3)\,T}\left(\dfrac{2}{3}T - t\right), & \dfrac{1}{3}T \leq t < \dfrac{2}{3}T \\ 0, & \dfrac{2}{3}T \leq t < T, \end{cases} \tag{11}$$

where ΔQ_{peak} and T are the peak value and cycle time of the disturbance, respectively.

The first two parts are the rise/fall or fall/rise sections of the symmetric triangular, respectively. Whether the rise section or the fall section starts first depends on the sign of ΔQ_{peak}. If ΔQ_{peak} is positive, the first part of the disturbance is the rise section of the triangular shape. In addition, the peak value and cycle time of the disturbance in this cycle can be calculated according to the frequency in the third part of the disturbance in the last cycle. As for the third part of the disturbance in a cycle, the disturbance value is set as zero. This part aims to obtain the value of f_1, which is the frequency without disturbance after islanding. Then, the peak value and cycle time of the disturbance in the next cycle can be calculated, which is introduced in detail afterwards.

In order to keep the frequency in its normal range during islanding and reduce the NDZ, the frequency corresponding to the peak value of the disturbance is set as the frequency threshold (50.5 Hz or 49.5 Hz). Therefore, if islanding occurs, the frequency will deviate from f_1 to its threshold, return back to f_1 afterwards, and repeat the abovementioned process periodically. As mentioned in Section 2, the peak value of the disturbance on the reactive power output will be within $\pm 5\% \, P_{DG}$ if proper threshold value is chosen for f_1. However, the peak value of the disturbance decreases along with the increasing value of f_1. If f_1 is close to the frequency threshold, the peak value of the disturbance will be small. The method might fail to detect islanding in this condition. Therefore, the frequency corresponding to the peak value of the disturbance is set as 50 Hz when f_1 is close to the frequency threshold (such as when f_1 is above 50.25 Hz or below 49.75 Hz). If islanding occurs in this condition, the frequency will deviate from f_1 to 50 Hz, return back to f_1 afterwards, and repeat the abovementioned process periodically. According to (8), the peak value of the disturbance can be calculated as follows for the DG operating at a unity power factor:

$$\Delta Q_{peak} = \begin{cases} P_{DG}Q_f\left(\dfrac{f_1}{50} - \dfrac{50}{f_1}\right), \\ \quad 50.5\,\text{Hz} \geq f_1 > 50.25\,\text{Hz} \\ P_{DG}Q_f\left(\dfrac{f_1}{50.5} - \dfrac{50.5}{f_1}\right), \\ \quad 50.25\,\text{Hz} \geq f_1 \geq 50\,\text{Hz} \\ P_{DG}Q_f\left(\dfrac{f_1}{49.5} - \dfrac{49.5}{f_1}\right), \\ \quad 49.75\,\text{Hz} \leq f_1 < 50\,\text{Hz} \\ P_{DG}Q_f\left(\dfrac{f_1}{50} - \dfrac{50}{f_1}\right), \\ \quad 49.5\,\text{Hz} \leq f_1 < 49.75\,\text{Hz}. \end{cases} \tag{12}$$

As for the DG generating the active and reactive power simultaneously, the peak value of the disturbance can be obtained as follows according to (10):

$$\Delta Q_{peak} = \begin{cases} P_{DG}Q_f\left(f_1 - 50\right)\left(\dfrac{1}{f_1} + \dfrac{1}{50}\right), \\ \quad 50.5\,\text{Hz} \geq f_1 > 50.25\,\text{Hz} \\ P_{DG}Q_f\left(f_1 - 50.5\right)\left(\dfrac{50}{50.5f_1} + \dfrac{1}{50}\right), \\ \quad 50.25\,\text{Hz} \geq f_1 \geq 50\,\text{Hz} \\ P_{DG}Q_f\left(f_1 - 49.5\right)\left(\dfrac{50}{49.5f_1} + \dfrac{1}{50}\right), \\ \quad 49.75\,\text{Hz} \leq f_1 < 50\,\text{Hz} \\ P_{DG}Q_f\left(f_1 - 50\right)\left(\dfrac{1}{f_1} + \dfrac{1}{50}\right), \\ \quad 49.5\,\text{Hz} \leq f_1 < 49.75\,\text{Hz}. \end{cases} \tag{13}$$

On the other hand, the cycle time of the disturbance should be properly designed as well. The design of the cycle time has two purposes: (1) minimizing the total amount of the disturbance; (2) making sure that the absolute value of the ROCOF is constant in the triangular parts of the disturbance when islanding occurs. Assuming that the cycle time is T_1 when f_1 is 50 Hz, the frequency deviates to 50.5 Hz after one-third of the cycle time T_1. Therefore, the absolute value of the ROCOF is equal to $1.5/T_1$ (Hz/s). If f_1 is not equal to 50 Hz, the cycle time of the disturbance can be obtained as follows:

$$T = \begin{cases} \dfrac{f_1 - 50}{50.5 - 50}T_1, & 50.5\,\text{Hz} \geq f_1 > 50.25\,\text{Hz} \\ \dfrac{50.5 - f_1}{50.5 - 50}T_1, & 50.25\,\text{Hz} \geq f_1 \geq 50\,\text{Hz} \\ \dfrac{f_1 - 49.5}{50 - 49.5}T_1, & 49.75\,\text{Hz} \leq f_1 < 50\,\text{Hz} \\ \dfrac{50 - f_1}{50 - 49.5}T_1, & 49.5\,\text{Hz} \leq f_1 < 49.75\,\text{Hz}. \end{cases} \tag{14}$$

It can be seen from (14) that the cycle time also depends on the value of f_1 and it changes adaptively to shorten the duration of the disturbance and keep the absolute value of the ROCOF equal to $1.5/T_1$.

The value of T_1 is preset. When the first part of the disturbance in a cycle starts, it is checked whether the absolute value of the ROCOF is equal to $1.5/T_1$ or not. If the absolute value of the ROCOF is equal to $1.5/T_1$ and the situation lasts for the time preset in advance, islanding will be nondestructively detected based on this criterion with the frequency in its allowable range. Assuming that P_{DG} is equal to 1 and T_1 is set as 0.3 s, the adaptive and periodic disturbance on the reactive power output of the DG with different values of f_1 is shown in Figure 4.

When the method is applied to multiple DGs, the effectiveness of the method based on above criterion depends on whether or not the disturbances on the reactive power output of DGs are synchronous. If the disturbances are synchronous, the criterion mentioned above will still be satisfied after islanding and islanding will be detected effectively. However, if the disturbances are asynchronous, the total amount of the disturbances will be inadequate to force the frequency
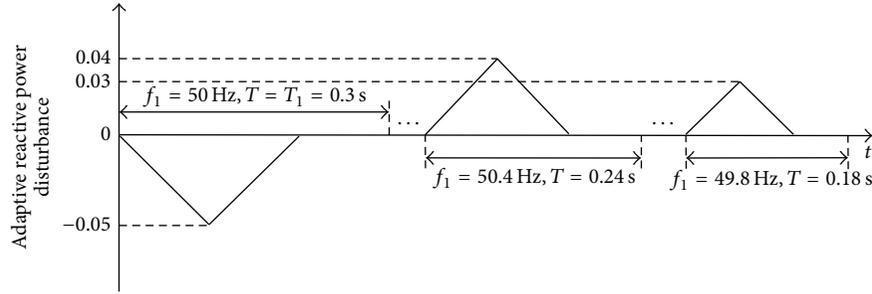
FIGURE 4: The adaptive and periodic disturbance with different values of f_1.

to deviate to its target value (50.5 Hz, 49.5 Hz, or 50 Hz). Accordingly, the absolute value of the ROCOF will be smaller than $1.5/T_1$. Therefore, additional criterion is needed for multiple-DG operation in case of the disturbance asynchrony based on the characteristic in this situation.

The values of f_1 calculated by DGs are the same after islanding because DGs are in the same islanding system. Therefore, the peak values and cycle time of the disturbances and the frequency's target value are the same as well. Moreover, according to the proposed method, the disturbance in a cycle is designed to have three parts with equal duration. Therefore, the frequency will deviate periodically after islanding and its cycle time is always equal to that of the disturbance no matter whether the disturbances are synchronous or not. This characteristic can be utilized as the additional criterion to detect islanding when the disturbances are asynchronous in multiple-DG operation. The detection time with this criterion is a little bit longer than that based on the absolute value of the ROCOF and its duration, but it is much shorter than 2 s as the IEEE standard required.

Therefore, both criterions are configured in the DG. If either one of both criterions is satisfied, islanding will be detected rapidly and effectively no matter whether the disturbances on the reactive power output of both DGs are synchronous or not.

4. Performance of the Proposed Method during Islanding

In this section, several study cases are simulated on the power systems computer-aided design (PSCAD)/EMTDC based on the system in Figure 1. The main system parameters are given in Table 1. Adopting the interface control presented in Figure 2, the DG performs as a constant power source. The designed disturbance is added on the reactive power output of the DG. The frequency is 50 Hz before islanding and T_1 is set as 0.3 s. The islanding is initiated at $t = 0.3$ s. The performance of the proposed islanding detection method is tested under different conditions.

4.1. Application on the DG Operating at a Unity Power Factor. To examine the performance of the proposed method when it is applied on the DG operating at a unity power factor, three test cases are designed with different values of RLC load as shown in Table 2. There are no active and reactive

TABLE 1: Parameters of the study system.

	Parameters	Values
	Voltage	400 V
Grid	Frequency	50 Hz
	Grid resistance	0.05 Ω
	Grid inductance	0.8 mH
	K_{p1}/K_{i1}	0.025/2
DG inverter controller	K_{p2}/K_{i2}	1.5/0.01
	P_{ref}	200 kW

TABLE 2: Parameters of the RLC load.

	Parameters	Case 1	Case 2	Case 3
	R	0.8 Ω	0.8 Ω	0.8 Ω
RLC load	L	1.0186 mH	1.0227 mH	1.0145 mH
	C	9947.2 μF	9987.1 μF	9907.6 μF
	f_0	50 Hz	49.8 Hz	50.2 Hz

power mismatches in Case 1. Only reactive power mismatch exists in Cases 2 and 3. The values of the load's resonant frequency f_0 in these three cases are different. The frequency is 50 Hz before islanding. Therefore, the disturbance, whose peak value and cycle time have been determined with f_1 equal to 50 Hz, will last for a while (not longer than a cycle) until the next cycle after islanding. Considering the unpredictability of its duration, two scenarios are simulated: (1) the third part of the disturbance in this cycle just starts; (2) the first part of the disturbance in this cycle is half completed. When the disturbance value in this cycle is equal to zero, the value of f_1 can be obtained again. Then, the peak value and cycle time of the disturbance in the next cycle can be calculated. For the DG operating at a unity power factor, the value of f_1 is equal to that of f_0 during islanding and the value of the DG reactive power output is equal to that of the disturbance as well.

For the first scenario, Figure 5 illustrates the PCC frequencies and the DG reactive power output of three cases, respectively. It can be seen from Figure 5 that the sudden change of the load reactive power consumption (from the rated reactive power consumption to 0 Var) in Cases 2 and 3 leads to transient processes of the frequencies. The values of f_1 in three cases are 50 Hz, 49.8 Hz, and 50.2 Hz, respectively. Accordingly, the peak values of the disturbance in the next cycle are −10 kVar (−5% P_{DG}), 6 kVar (3% P_{DG}),
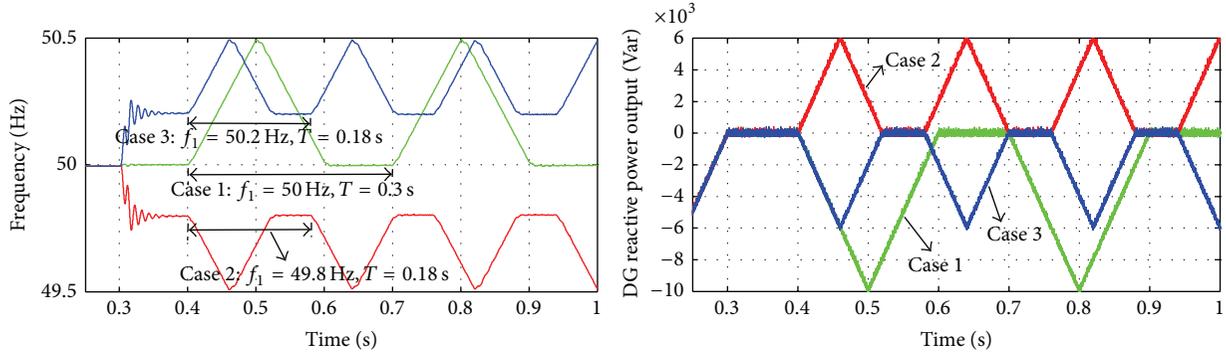
Figure 5: The PCC frequencies and reactive power output of the DG in the first scenario.
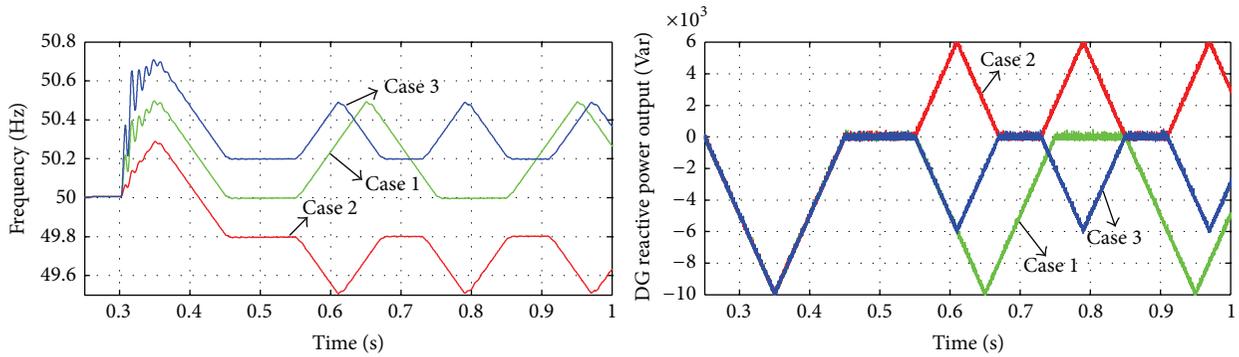

Figure 6: The PCC frequencies and reactive power output of the DG in the second scenario.

and -6 kVar ($-3\%P_{DG}$) and cycle time is 0.3 s, 0.18 s, and 0.18 s. Corresponding to the first two parts of the disturbance in a cycle, the frequency is forced to deviate in a triangular shape. When the first part of the disturbance in a cycle starts, it is checked whether the absolute value of the ROCOF is equal to 5 (Hz/s) or not. If the absolute value of the ROCOF is equal to 5 and the situation lasts for 10 ms, islanding is detected nondestructively. Islanding can be detected within 110 ms for three cases in this scenario. Afterwards, when the disturbance value is equal to zero, the control strategy transformation of the DG for microgrid islanded operation can be implemented to avoid the serious transient process.

Figure 6 illustrates the PCC frequencies and the DG reactive power output of three cases for the second scenario, respectively. When islanding occurs, the peak value and cycle time of the disturbance at that time have been determined according to the normal system frequency 50 Hz. They will not change until the next disturbance period for all the three cases. For both Cases 1 and 2, where the values of f_1 are not larger than 50 Hz, the frequencies are within the normal range after islanding and islanding detection time is within 60 ms. However, the value of f_1 in Case 3 is 50.2 Hz and the maximum frequency after islanding reaches up to 50.7 Hz, which corresponds to the peak value of the disturbance calculated according to 50 Hz. The frequency deviates outside its upper threshold 50.5 Hz and the passive OFP/UFP method can detect islanding within 50 ms. The DG transforms its

control strategy for microgrid islanded operation when the disturbance value is equal to zero for three cases.

For the situations like Case 3 in the second scenario, the maximum frequency should be as small as possible to make the power quality better. In order to realize this target, the proposed method can be further improved. When the frequency is detected to just begin to be above 50.5 Hz, the value of the disturbance at that time ΔQ_{thr} is captured. Then, the value of the disturbance is maintained to be ΔQ_{thr} for a while. The duration of this situation can be calculated as follows:

$$t = \left(\frac{2T}{3}\right)\left(\frac{\Delta Q_{peak} - \Delta Q_{thr}}{\Delta Q_{peak}}\right). \tag{15}$$

According to the improved method, the PCC frequencies and the DG reactive power output of three cases in the second scenario are shown in Figure 7. Compared with the frequency of Case 3 as shown in Figure 6, it is approximately equal to 50.5 Hz after the transient process. Therefore, the improved method can guarantee the better power quality for the situations like Case 3 in the second scenario.

4.2. Application on the DG Generating Active and Reactive Power Simultaneously. This part aims to verify the effectiveness of the proposed method when it is applied on the DG generating active and reactive power simultaneously. As
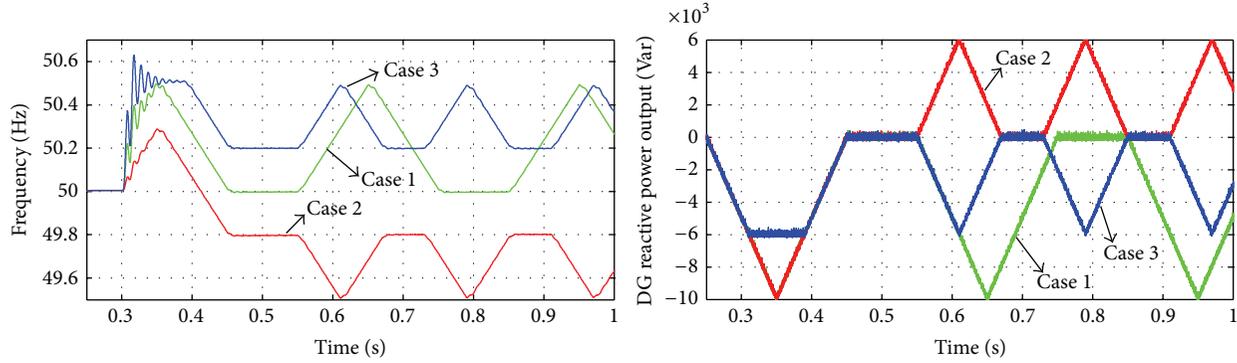
FIGURE 7: The PCC frequencies and reactive power output of the DG in the second scenario with the improved method.
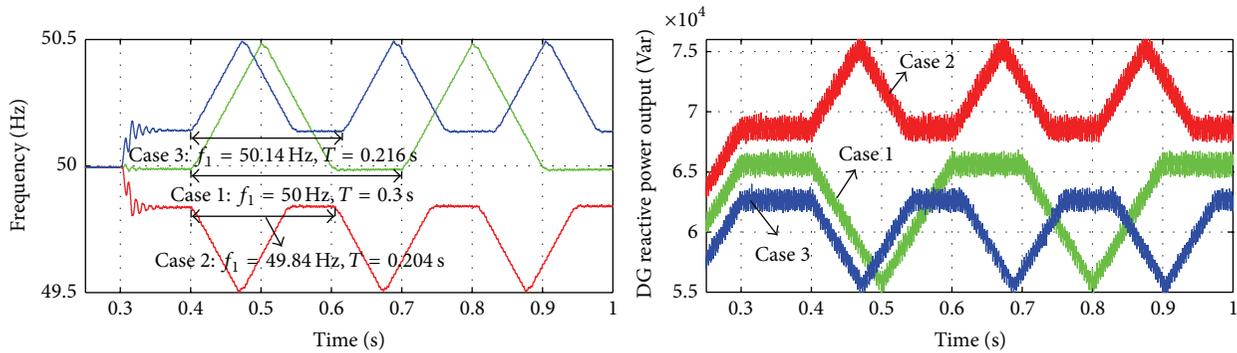

FIGURE 8: The PCC frequencies and reactive power output of the DG in the first scenario.

TABLE 3: Parameters of the RLC load and DG reactive power output without the disturbance.

	Parameters	Case 1	Case 2	Case 3
	R	0.8 Ω	0.8 Ω	0.8 Ω
RLC load	L	0.9539 mH	0.9539 mH	0.9539 mH
	C	9315.03 μF	9315.03 μF	9315.03 μF
DG reactive power output	Q	65.74 kVar	68.74 kVar	62.74 kVar

shown in Table 3, three test cases are also designed with different values of DG reactive power output. These values are the DG reactive power output without considering the disturbance. The RLC load's power factor is set to 0.95 with the rated active and reactive power equal to 200 kW and 65.74 kVar, respectively. Therefore, the values of f_1 are different in these three cases due to different reactive power mismatches. Like in Section 4.1, the two scenarios are simulated as well in this part.

Figure 8 illustrates the PCC frequencies and the DG reactive power output of three cases in the first scenario. The values of f_1 of three cases are 50 Hz, 49.84 Hz, and 50.14 Hz, respectively. Accordingly, the peak values of the disturbances in the next cycle are −10 kVar (−5% P_{DG}), 6.8 kVar (3.4% P_{DG}), and −7.2 kVar (−3.6%P_{DG}) and the cycle time of the disturbances is 0.3 s, 0.204 s, and 0.216 s. Moreover, it can be seen that the absolute values of the ROCOF in three cases are equal to 5 (Hz/s) when the first parts of the disturbances in the next cycle start after islanding, and the duration of these

situations is over 10 ms. Therefore, islanding can be detected effectively within 110 ms in these three test cases.

On the other hand, Figure 9 illustrates the PCC frequencies and the DG reactive power output of three cases in the second scenario, respectively. Like the second scenario in Section 4.1, the frequencies of Cases 1 and 2 are within their normal ranges. The absolute values of the ROCOF are equal to 5 (Hz/s) during the second parts of the disturbances after islanding, and the duration of these situations is over 10 ms. Therefore, islanding can be detected effectively within 60 ms in Cases 1 and 2. In addition, the frequency of Case 3 deviates outside its upper threshold and islanding can be detected by the passive OFP/UFP method. The value of the frequency is approximately equal to 50.5 Hz after the transient process with the improved method and the frequency is kept within its normal range afterwards.

4.3. Multiple-DG Operation. According to the simulation results in Sections 4.1 and 4.2 the methods can detect
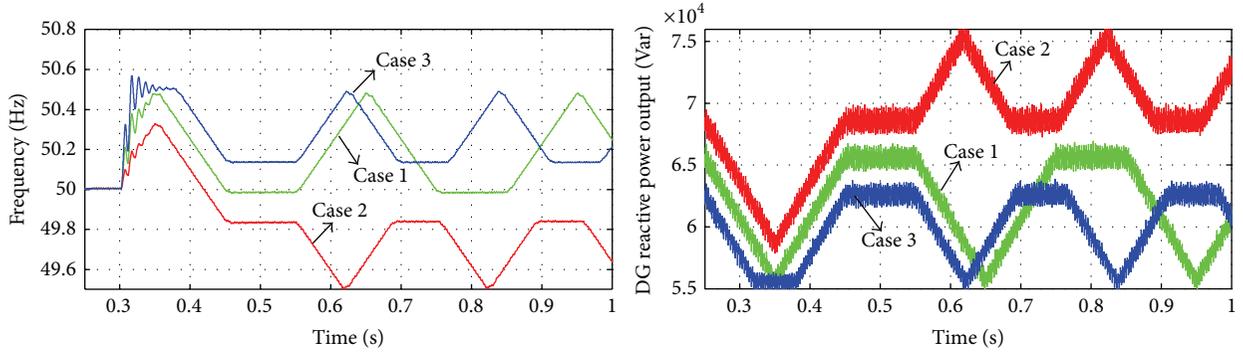
FIGURE 9: The PCC frequencies and reactive power output of the DG in the second scenario with the improved method.
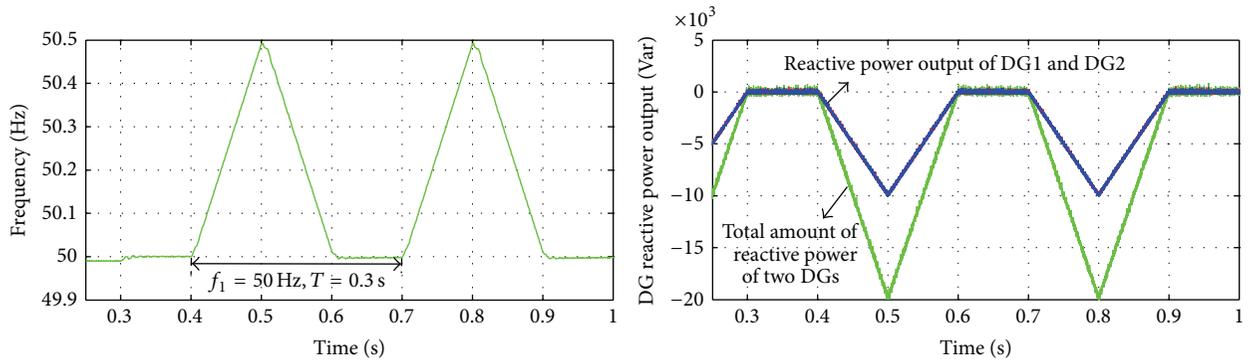

FIGURE 10: The PCC frequency and the separate and total reactive power output of both DGs in the first scenario.

islanding effectively for the DG either operating at a unity power factor or generating active and reactive power simultaneously in both scenarios. Therefore, the performance of the proposed method is only tested on the system with both DGs operating at a unity power factor in this part. Both DGs connect with their own local load, respectively, and then connect together at the PCC. The parameters of the local RLC load are the same with those in Case 1 of Section 4.1. Moreover, considering that the disturbances on the reactive power output of both DGs might be asynchronous, two scenarios are simulated as well in this part: (1) the disturbances on the reactive power output of both DGs are synchronous; (2) the disturbance on the reactive power output of one DG lags by 0.03 s (0.1T) behind that on the reactive power output of the other one.

Figure 10 presents the frequency and the separate and total reactive power output of both DGs in the first scenario, respectively. Due to the disturbance synchronization, the frequency can deviate to its threshold 50.5 Hz and the absolute value of the ROCOF is equal to 5 (Hz/s). Therefore, islanding can be detected within 110 ms for this scenario.

Figure 11 presents the frequency and the separate and total reactive power output of both DGs in the second scenario, respectively. When islanding occurs, there is a sudden change of the load reactive power consumption (from 0 Var to the current value of the total reactive power). Therefore, the frequency goes through a transient process. In addition, the total amount of the disturbances is inadequate to force

the frequency to deviate to 50.5 Hz because the disturbances on the reactive power output of both DGs are asynchronous. It can be seen from Figure 11 that when the triangular wave parts of the disturbances start, the frequency deviates periodically with the cycle time equal to 0.3 s. Islanding can be detected within 400 ms for this scenario, which is still far less than the 2 s as the standard required.

5. Conclusion

According to the relationship between the reactive power mismatch and the frequency deviation, a nondestructive islanding detection method based on adaptive and periodic disturbance on the reactive power output of the DG is proposed in this paper. The disturbance in a cycle is designed to have three parts. The first two parts form a symmetric triangular shape. Accordingly, the frequency deviates in a symmetric triangular shape when islanding occurs. This design guarantees that the frequency is within its normal range during islanding. The value of the third part of the disturbance is equal to zero. According to the frequency in this part, the disturbance in the next cycle can adaptively adjust its peak value and cycle time.

Therefore, the total amount of the disturbance is the minimum. The absolute value of the ROCOF is constant during islanding, which can be utilized to be a criterion to detect islanding rapidly. Afterwards, when the disturbance value is equal to zero, the control strategy transformation of
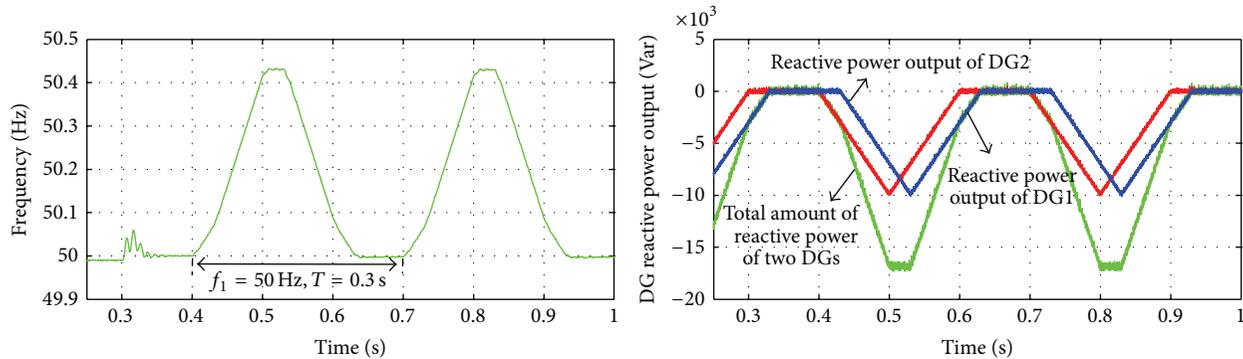
FIGURE 11: The PCC frequency and the separate and total reactive power output of both DGs in the second scenario.

the DG for microgrid islanded operation can be implemented to avoid the serious transient process. In addition, the method has the universal nature. It can be applied on the DG either operating at a unity power factor or generating both active and reactive power simultaneously. Furthermore, it also performs effectively for the system with multiple DGs.

Conflict of Interests

The authors declare that there is no conflict of interests regarding the publication of this paper.

Acknowledgments

References

[1] H. B. Püttgen, P. R. Macgregor, and F. C. Lambert, "Distributed generation: semantic hype or the dawn of a new era ?" *IEEE Power & Energy Magazine*, vol. 1, no. 1, pp. 22–29, 2003.

[2] R. H. Lasseter, "MicroGrids," in *Proceedings of the IEEE Power Engineering Society Winter Meeting (PESWM '02)*, pp. 305–308, New York, NY, USA, January 2002.

[3] R. H. Lasseter, "CERTS microgrid," in *Proceedings of the IEEE International Conference on System of Systems Engineering (SOSE '07)*, pp. 1–5, San Antonio, Tex, USA, April 2007.

[4] R. H. Lasseter, "Extended CERTS microgrid," in *Proceedings of the IEEE Power and Energy Society General Meeting (PESGM '08)*, pp. 1–5, July 2008.

[5] P. P. Barker and R. W. de Mello, "Determining the impact of distributed generation on power systems: part 1—Radial distribution systems," in *Proceedings of IEEE Power Engineering Society Summer Meeting (PESSM '00)*, pp. 1645–1656, July 2000.

[6] R. S. Al Abri, E. F. El-Saadany, and Y. M. Atwa, "Optimal placement and sizing method to improve the voltage stability margin in a distribution system using distributed generation," *IEEE Transactions on Power Systems*, vol. 28, no. 1, pp. 326–334, 2013.

[7] IEEE, "Recommended practice for utility interface of photovoltaic (PV) systems," IEEE Standard 929-2000, 2000.

[8] "IEEE Standard for Interconnecting Distributed Resources with Electric Power Systems," IEEE Standard 1547-2003, July 2003.

[9] I. J. Balaguer, Q. Lei, S. T. Yang, U. Supatti, and F. Z. Peng, "Control for grid-connected and intentional islanding operations of distributed power generation," *IEEE Transactions on Industrial Electronics*, vol. 58, no. 1, pp. 147–157, 2011.

[10] R. A. Walling and N. W. Miller, "Distributed generation islanding—implications on power system dynamic performance," in *Proceedings of the IEEE Power Engineering Society Summer Meeting (PESSM '02)*, pp. 92–96, July 2002.

[11] A. Timbus, A. Oudalov, and C. N. M. Ho, "Islanding detection in smart grids," in *Proceedings of the IEEE Energy Conversion Congress and Exposition (ECCE '10)*, pp. 3631–3637, Atlanta, Ga, USA, September 2010.

[12] F. de Mango, M. Liserre, A. Dell'Aquila, and A. Pigazo, "Overview of anti-islanding algorithms for PV systems. Part I: passive methods," in *Proceedings of the 12th International Power Electronics and Motion Control Conference (PEMC '06)*, pp. 1878–1883, Portoroz,Slovenia, September 2006.

[13] "Technical Requirements for Grid Connection of PV System," Chinese Standard GB19939-2005, November 2005.

[14] Z. Ye, A. Kolwalkar, Y. Zhang, P. Du, and R. Walling, "Evaluation of anti-islanding schemes based on nondetection zone concept," *IEEE Transactions on Power Electronics*, vol. 19, no. 5, pp. 1171–1176, 2004.

[15] F. de Mango, M. Liserre, and A. Dell'Aquila, "Overview of anti-islanding algorithms for PV systems. Part II: active methods," in *Proceedings of the 12th International Power Electronics and Motion Control Conference (PEMCC '06)*, pp. 1884–1889, August-September 2006.

[16] J. H. Kim, J. G. Kim, Y. H. Ji, Y. C. Jung, and C. Y. Won, "An islanding detection method for a grid-connected system based on the goertzel algorithm," *IEEE Transactions on Power Electronics*, vol. 26, no. 4, pp. 1049–1055, 2011.

[17] H. Karimi, A. Yazdani, and R. Iravani, "Negative-sequence current injection for fast islanding detection of a distributed resource unit," *IEEE Transactions on Power Electronics*, vol. 23, no. 1, pp. 298–307, 2008.

[18] A. Yafaoui, B. Wu, and S. Kouro, "Improved active frequency drift anti-islanding detection method for grid connected photovoltaic systems," *IEEE Transactions on Power Electronics*, vol. 27, no. 5, pp. 2367–2375, 2012.

[19] L. A. C. Lopes and H. L. Sun, "Performance assessment of active frequency drifting islanding detection methods," *IEEE Transactions on Energy Conversion*, vol. 21, no. 1, pp. 171–180, 2006.

[20] H. Vahedi and M. Karrari, "Adaptive fuzzy Sandia frequency-shift method for islanding protection of inverter-based distributed generation," *IEEE Transactions on Power Delivery*, vol. 28, no. 1, pp. 84–92, 2013.

[21] E. J. Estebanez, V. M. Moreno, A. Pigazo, M. Liserre, and A. Dell'Aquila, "Performance evaluation of active islanding-detection algorithms in distributed-generation photovoltaic systems: two inverters case," *IEEE Transactions on Industrial Electronics*, vol. 58, no. 4, pp. 1185–1193, 2011.

[22] L. A. C. Lopes and Y. Z. Zhang, "Islanding detection assessment of multi-inverter systems with active frequency drifting methods," *IEEE Transactions on Power Delivery*, vol. 23, no. 1, pp. 480–486, 2008.

[23] Y. Jin, Q. Song, and W. Liu, "Anti-islanding protection for distributed generation systems based on reactive power drift," in *Proceedings of the 35th Annual Conference of the IEEE Industrial Electronics (IECON '09)*, pp. 3970–3975, Porto, Portugal, November 2009.

[24] H. H. Zeineldin, "A *Q-f* droop curve for facilitating islanding detection of inverter-based distributed generation," *IEEE Transactions on Power Electronics*, vol. 24, no. 3, pp. 665–673, 2009.

[25] J. Zhang, D. Xu, G. Shen, Y. Zhu, N. He, and J. Ma, "An improved islanding detection method for a grid-connected inverter with intermittent bilateral reactive power variation," *IEEE Transactions on Power Electronics*, vol. 28, no. 1, pp. 268–278, 2013.

[26] Y. Zhu, D. Xu, N. He et al., "A novel RPV (Reactive-Power-Variation) antiislanding method based on adapted reactive power perturbation," *IEEE Transactions on Power Electronics*, vol. 28, no. 11, pp. 4998–5012, 2013.

[27] P. G. Barbosa, L. G. B. Rolim, E. H. Watanabe, and R. Hanitsch, "Control strategy for grid-connected DC-AC converters with load power factor correction," *IEE Proceedings—Generation, Transmission and Distribution*, vol. 145, no. 5, pp. 487–491, 1998.

[28] S.-J. Huang and F. Pai, "Design and operation of grid-connected photovoltaic system with power-factor control and active islanding detection," *IEE Proceedings: Generation, Transmission and Distribution*, vol. 148, no. 3, pp. 243–250, 2001.

[29] E. Demirok, D. Sera, R. Teodorescu, P. Rodriguez, and U. Borup, "Evaluation of the voltage support strategies for the low voltage grid connected PV generators," in *Proceedings of the 2nd IEEE Energy Conversion Congress and Exposition (ECCE '10)*, pp. 710–717, September 2010.

[30] M. A. Kashem and G. Ledwich, "Distributed generation as voltage support for single wire earth return systems," *IEEE Transactions on Power Delivery*, vol. 19, no. 3, pp. 1002–1011, 2004.

[31] H. H. Zeineldin, E. F. El-Saadany, and M. M. A. Salama, "Islanding detection of inverter-based distributed generation," *IEE Proceedings: Generation, Transmission and Distribution*, vol. 153, no. 6, pp. 644–652, 2006.

[32] C. Schauder and H. Mehta, "Vector analysis and control of advanced static VAR compensators," *IEE Proceedings C: Generation Transmission and Distribution*, vol. 140, no. 4, pp. 299–306, 1993.

[33] H. H. Zeineldin, E. F. El-Saadany, and M. M. A. Salama, "Impact of DG interface control on islanding detection and nondetection zones," *IEEE Transactions on Power Delivery*, vol. 21, no. 3, pp. 1515–1523, 2006.

[34] X. Chen and Y. Li, "An islanding detection algorithm for inverter-based distributed generation based on reactive power control," *IEEE Transactions on Power Electronics*, vol. 29, no. 9, pp. 4672–4683, 2014.